The Astrophysical Journal, 862:134 (7pp), 2018 August 1 https://doi.org/10.3847/1538-4357/aacc69

Electron–ion Recombination Rate Coefficients of Be-like $^{40}Ca^{16+}$

S. X. Wang[1,2], X. Xu[1,2], Z. K. Huang[3], W. Q. Wen[3], H. B. Wang[3], N. Khan[3], S. P. Preval[4], N. R. Badnell[5], S. Schippers[6], S. Mahmood[3,7], L. J. Dou[3], X. Y. Chuai[3], D. M. Zhao[3], X. L. Zhu[3], L. J. Mao[3], X. M. Ma[3], J. Li[3], R. S. Mao[3], Y. J. Yuan[3], M. T. Tang[3], D. Y. Yin[3], J. C. Yang[3], X. Ma[3], and L. F. Zhu[1,2]

[1] Hefei National Laboratory for Physical Sciences at Microscale and Department of Modern Physics, University of Science and Technology of China, Hefei, Anhui 230026, People's Republic of China; lfzhu@ustc.edu.cn

[2] Synergetic Innovation Center of Quantum Information and Quantum Physics, University of Science and Technology of China, Hefei, Anhui 230026, People's Republic of China

[3] Institute of Modern Physics, Chinese Academy of Sciences, 730000 Lanzhou, People's Republic of China; wenweiqiang@impcas.ac.cn, x.ma@impcas.ac.cn

[4] Department of Physics and Astronomy, University of Leicester, University Road, Leicester, LE1 7RH, UK

[5] Department of Physics, University of Strathclyde, Glasgow G4 0NG, UK

[6] I. Physikalisches Institut, Justus-Liebig-Universität Gießen, Heinrich-Buff-Ring 16, D-35392 Giessen, Germany

[7] Physics Division, PINSTECH, Nilore, Islamabad, 45650, Pakistan

Received 2018 May 17; revised 2018 June 9; accepted 2018 June 11; published 2018 July 31

Abstract

Electron–ion recombination rate coefficients for beryllium-like calcium ions in the center of mass energy from 0 to 51.88 eV have been measured by means of the electron–ion merged-beam technique at the main cooler storage ring at the Institute of Modern Physics in Lanzhou, China. The measurement energy range covers the dielectronic recombination (DR) resonances associated with the $2s^2\ ^1S_0 \rightarrow 2s2p\ ^3P_{0,1,2}$, $^1P_1$ core excitations and the trielectronic recombination (TR) resonances associated with the $2s^2\ ^1S_0 \rightarrow 2p^2\ ^3P_{0,1,2}$, $^1D_2$, $^1S_0$ core excitations. In addition, the AUTOSTRUCTURE code was used to calculate the recombination rate coefficients for comparison with the experimental results. Resonant recombination originating from parent ions in the long-lived metastable state $2s2p\ ^3P_0$ ions has been identified in the recombination spectrum below 1.25 eV. A good agreement is achieved between the experimental recombination spectrum and the result of the AUTOSTRUCTURE calculations when fractions of 95% ground-state ions and 5% metastable ions are assumed in the calculation. It is found that the calculated TR resonance positions agree with the experimental peaks, while the resonance strengths are underestimated by the theoretical calculation. Temperature dependent plasma rate coefficients for DR and TR in the temperature range of 10^3–10^8 K were derived from the measured electron–ion recombination rate coefficients and compared with the available theoretical results from the literature. In the temperature range of photoionized plasmas, the presently calculated rate coefficients and the recent results of Gu & Colgan et al. are up to 30% lower than the experimentally derived ones, and the older atomic data are even up to 50% lower than the present experimental result. This is because strong resonances situated below electron–ion collision energies of 50 meV were underestimated by the theoretical calculation, which also has a severe influence on the rate coefficients in low-temperature plasmas. In the temperature range of collisionally ionized plasmas, agreement within 25% was found between the experimental result and the present calculation as well as the calculation by Colgan et al. The present result constitutes a set of benchmark data for use in astrophysical modeling.

Key words: atomic data – atomic processes – plasmas

1. Introduction

Plasma is the most abundant form of visible matter in the universe (Beyer & Shevelko 2003). Cosmic atomic plasmas are often divided into two broad classes (see Savin 2007, for a more in-depth discussion): (i) photoionized plasmas (PP), often found in planetary nebulae, X-ray binaries, cold nova shells, and active galactic nuclei (AGNs); (ii) collisionally ionized plasmas (CP), often found in the Sun, stars, supernova remnants and galaxies. Electron–ion collision processes, such as electron impact ionization, excitation, de-excitation and electron–ion recombination, can result in the emission of radiation. In order to explore the properties of astrophysical plasmas, such as, e.g., charge state distribution, temperature, and relative elemental abundances (Beiersdorfer 2003; Kallman & Palmeri 2007), the X-ray observatories *Chandra* (NASA), Hinode (NASA), and XMM-Newton (ESA), have been launched to collect high resolution X-ray spectra from various cosmic sources (Paerels & Kahn 2003). To interpret the observed spectra by plasma modeling, accurate electron–ion recombination data, in particular, for radiative recombination (RR) and dielectronic recombination (DR), are crucial for astrophysicists.

The significance of DR in plasma was not appreciated until Burgess first recognized its importance in 1964 (Burgess 1964). Since then, DR has been considered to be a significant electron–ion recombination mechanism, governing the charge state distribution and the temperature in atomic plasmas and contributing to their line emission (Badnell 2007; Savin 2007). Reliable recombination rate coefficients are required for understanding and modeling laboratorial or astrophysical plasmas. Most of the available rate coefficients are from theory. However, the theoretical prediction of DR resonance positions and strengths, particularly at low electron–ion collision energies, is still a challenging task since an infinite number of states is involved in the DR process and relativistic many-body effects should be taken into account in high orders. Presently available atomic-structure codes are not able to provide resonance positions in the low energy region with sufficient precision. Unfortunately, small shifts of low energy

DR resonance positions can translate into huge uncertainties of the temperature dependent rate coefficient in a plasma (Schippers et al. 2004). In addition, recent experimental studies of low energy range DR have also shown that results from earlier computations of low-temperature DR rate coefficients are not reliable (Huang et al. 2018). Thus, accurate experimental DR rate coefficients are needed to benchmark different theoretical approaches and to produce more reliable recombination data. It should be noted that heavy-ion storage rings equipped with electron coolers are presently the only tools to produce reliable low-temperature DR rate coefficients with high precision. Details about storage ring DR experiments (Schuch & Böhm 2007; Schippers 2015; Brandau et al. 2015) have been reviewed by Schippers (2012). Several successful DR experiments have been carried out at the main cooler storage ring (CSRm) at the Institute of Modern Physics (IMP), Lanzhou, China (Huang et al. 2015, 2018; Khan et al 2018).

Calcium is one of the most abundant elements in the solar system (Feldman & Laming 2000; Asplund et al. 2009) and the solar element abundances reflect the element abundances in the universe (Doschek & Feldman 2010). Extreme ultraviolet transitions of Ca XVI have been identified in the solar flare spectra and studied in the laboratory (Keenan et al. 1998). Line emissions caused by $2s2p\ ^1P_1 - 2s^2\ ^1S_0$ transition of Ca XVII at 192.8 Å were widely observed in X-ray solar flare spectra by the Extreme-Ultraviolet Imaging Spectrometer (EIS) on Hinode (Ko et al. 2009). Observation of the Tycho supernova remnant by XMM-Newton and Cassiopeia A by *Chandra* have also revealed strong emissions from the calcium ions (Decourchelle et al. 2001; Hwang & Laming 2003). A summary of the spectral lines for Ca XVII can be found in the atomic data table compiled by Landi & Bhatia (2009). In addition, laboratory studies of the spectra of highly ionized calcium in the 100–250 Å range applied to solar flare diagnostics were performed at the TEXT tokamak (Lippmann et al. 1987). The solar UV–X-ray spectrum including lines associated Ca XVI and Ca XVII have been reviewed by Doschek & Feldman (2010). Here, we present the absolute electron–ion recombination rate coefficients for Be-like calcium ions from a storage ring experiment as well as a theoretical calculation with the AUTOSTRUCTURE code (Badnell 2011).

The measurement covers the range of collision energy from 0 to 51.88 eV, including the following recombination channels for the parent ions at the ground level:

$$\mathrm{Ca}^{16+}(2s^2[^1S_0]) + e^- \rightarrow \begin{cases} \mathrm{Ca}^{15+}(2s^2nl) + \gamma, \text{ RR;} \\ \mathrm{Ca}^{15+}(2s2p[^3P_{0,1,2};\ ^1P_1]nl)^{**} \rightarrow \mathrm{Ca}^{15+} + \gamma, \text{ DR;} \\ \mathrm{Ca}^{15+}(2p^2[^3P_{0,1,2};\ ^1D_2;\ ^1S_0]nl)^{***} \rightarrow \mathrm{Ca}^{15+} + \gamma, \text{ TR.} \end{cases} \quad (1)$$

Here γ denotes the decay photons. RR is the time reversal of direct photoionization, where an ion recombines with a free electron and the excess energy is emitted in the form of a photon simultaneously. DR is a two-step resonant process, in which a free electron is captured by an ion with a core electron excited simultaneously, forming a doubly excited ion at first. Subsequently, the unstable intermediate state decays either by autoionization or radiatively. The autoionization channel returns the system to the original charge state, whereas the radiative decay, when leading to a state below the ionization threshold, completes the DR process. In Be-like systems, due to the strong correlation between the two bound $2s$ electrons, they can be excited simultaneously forming triply excited $2p^2\ nl$ levels with the initially free electron being captured to an atomic subshell nl. As there are three electrons associated with this process and a triply excited state is formed, it is termed trielectronic recombination (TR). The transition energies and lifetimes associated with the channels discussed here are listed in Table 1.

Table 1
Energy Levels and Associated Lifetimes for $^{40}Ca^{16+}$ ion

Level	Excitation Energy		Lifetime
	NIST[a] (eV)	(Wang et al. 2015) (eV)	(Wang et al. 2015) (s)
$1s^22s^2\ ^1S_0$	0	0	∞
$1s^22s2p\ ^3P_0$	32.024	32.0355	2.3[6][b]
$1s^22s2p\ ^3P_1$	33.409	33.4235	1.475[−7]
$1s^22s2p\ ^3P_2$	36.817	36.8259	3.600[−3]
$1s^22s2p\ ^1P_1$	64.301	64.2983	8.948[−11]
$1s^22p^2\ ^3P_0$	85.435	85.4478	1.231[−10]
$1s^22p^2\ ^3P_1$	87.617	87.6299	1.148[−10]
$1s^22p^2\ ^3P_2$	90.068	90.0797	1.146[−10]
$1s^22p^2\ ^1D_2$	98.956	98.9378	3.325[−10]
$1s^22p^2\ ^1S_0$	119.914	119.903	5.736[−11]

Notes.
[a] Energy levels taken from NIST atomic spectra database (Kramida et al. 2018).
[b] Lifetime of the $2s2p\ ^3P_0$ level is estimated according to the calculated E1M1 two-photon transition rates (Fritzsche et al. 2015).

Previous DR experiments with several Be-like ions have been performed at heavy-ion storage rings. Electron–ion recombination rate coefficients of C^{2+}, N^{3+}, O^{4+} (Fogle et al. 2005), F^{5+} (Ali et al. 2013), Ne^{6+} (Orban et al. 2008), Mg^{8+} (Schippers et al. 2004), Si^{10+} (Orban et al. 2010; Bernhardt et al. 2016), Ar^{14+} (Huang et al. 2017, 2018), and Fe^{22+} (Savin et al. 2006) have been measured as benchmark data for astrophysical plasma modeling. TR was first observed with Be-like Cl^{13+} at the TSR (Schnell et al. 2003). Remarkably hyperfine-induced transition rates of Be-like Ti^{18+} and S^{12+} were investigated by means of DR spectroscopy at the TSR (Schippers et al. 2007a, 2007b; Schippers et al. 2012). Furthermore, DR spectroscopy was used to investigate quantum electrodynamics (QED) and electron–electron correlation effects in Ge^{28+} and Xe^{50+} (Orlov et al. 2009; Bernhardt et al. 2015).

Here we report the first laboratory measurement of the electron–ion recombination rate coefficients of Be-like calcium ions at the CSRm. The paper is structured as follows: Section 2 presents the experimental procedures and the data analysis. Section 3 gives a brief introduction of the theoretical calculation. Recombination rate coefficients are presented and compared with literature data in Section 4. Conclusions and the most important results are given in Section 5.

2. Experiment and Data Analysis

The experiment was carried out at the CSRm. The experimental setup and procedures have already been described by Huang et al. (2015, 2018). Here we will only give a brief introduction of the DR experiment with $^{40}Ca^{16+}$ ions.

During the experiment, a superconducting electron cyclotron resonance (ECR) ion source was used to produce the $^{40}Ca^{16+}$ ions. The produced ions were accelerated by a sector-focused cyclotron and then injected into the CSRm at an energy of 8.42 MeV/u. Every injection pulse of ions was sufficient to provide a maximum ion beam current of about 90 μA, corresponding to 1.4×10^8 ions stored in the ring. The storage lifetime of the ion beam was about 50 s. The designed 35 kV electron cooler was used to produce a cold electron beam to cool the ion beam as well as an electron target in the electron–ion recombination experiment. The effective interaction length L for the merged beams was 4.0 m. In order to generate a colder electron beam to reach a higher experimental resolution, it was magnetically expanded (Danared 1993). The magnetic fields applied at the cathode and the cooler section were 125 mT and 39 mT, respectively. The expanded diameter of the electron beam was $d \sim 62$ mm and the electron density in the cooler section was 9.2×10^5 cm^{-3}. Since the charge–mass ratio of the recombined ions is different from the parent ions, it will be separated from the primary ion beam at the dipole magnet. A movable scintillation detector (YAP: Ce+PMT) was placed at the first dipole magnet downstream from the electron cooler to detect the recombined ions with a nearly 100% efficiency (Wen et al. 2013).

To ensure a high ion beam quality, the stored ions were electron-cooled for about 2 s after their injection pulses into the storage ring. During the electron cooling, the electron energy was set at the cooling energy of 4.62 keV, which corresponds to zero electron–ion collision energy in the center of mass frame. Offset voltages were applied to the cathode voltage by a suitably designed detuning system to obtain nonzero collision energies. In addition, a beam diagnostic system was applied to monitor the electron and ion beams: ion beam currents were recorded by a DC current transformer in real time; one electron beam position monitor (BPM) and two ion BPMs were used to monitor the spatial overlap of the electron beam and the ion beam over the interaction section; the momentum spread of the ion beam was analyzed from the Schottky-noise signals recorded by a Tektronix RSA3408 spectrum analyzer. The latter was $\Delta p/p \sim 2.2 \times 10^{-4}$.

The absolute recombination rate coefficient as a function of the collision energy can be deduced from the energy dependent detector count rate $R(E)$ as

$$\alpha(E) = \frac{R(E)}{N_i n_e (1 - \beta_e \beta_i)} \frac{C}{L}. \quad (2)$$

Here, N_i is the number of the stored ions in the ring, n_e is the electron density, $C = 161.0$ m and $L = 4.0$ m denote the circumference of the ring and the length of the effective interaction section, respectively. RR and DR evolve from the same initial charge state to the same final charge state and they are indistinguishable quantum mechanically. Therefore, the deduced rate coefficient comprises of these two parts as well as a background resulting from collisions of stored ions with residual-gas particles. In this work, the RR rate coefficient and the background were subtracted by an empirical formula described by Schippers et al. (2000).

The electron–ion collision energy in the center of mass frame was calculated using

$$E_{\rm rel} = \sqrt{m_e^2 c^4 + m_i^2 c^4 + 2 m_e m_i \gamma_e \gamma_i c^4 (1 - \beta_e \beta_i \cos\theta)} - m_e c^2 - m_i c^2, \quad (3)$$

where m_e and m_i are the electron and ion rest mass, respectively, c is the speed of light, $\beta_e = \upsilon_e/c$ and $\beta_i = \upsilon_i/c$ are the electron and ion velocities in the laboratory frame, and γ_e and γ_i denote the respective Lorentz factors. The angle θ between the electron and ion beam is considered to be zero in the present experiment. Space charge effects were taken into account. Drag force effects were found to be negligible. The measurement covers the electron–ion collision energies in the center of mass frame ranging from 0 to 51.88 eV, which corresponds to detuning voltages in the range of 0–900 V. In the present experiment, the same power supplies were used as in the recombination experiment with Be-like Ar^{14+} at CSRm. Thus, the electron–ion collision energies derived from the detuning voltages have been rescaled by multiplying a factor of 1.05 in the same manner as described by Huang et al. (2018).

3. Theory

For a complete interpretation of the measured electron–ion recombination spectrum, the resonant recombination cross sections were calculated by the distorted-wave collision package AUTOSTRUCTURE (Badnell 2011), which is a versatile code to calculate energy levels, oscillator strengths, radiative/autoionization rates, and many other quantities using semi-relativistic kappa-averaged wave functions. The calculations for Ca^{16+} were performed in the same way as for Ar^{14+} (see Huang et al. 2018, for further details). In particular, the core excited energies were adjusted to match the spectroscopic values from the NIST atomic spectra database (Kramida et al. 2018). Fractions of 95% ground-state ions and 5% metastable ions were assumed in the calculation.

For a direct comparison of the measured rate coefficients with the theoretical calculation, the calculated cross sections were multiplied by the electron velocity and convoluted with the velocity distribution of the electrons for the experiment:

$$\alpha(E) = \int_{-\infty}^{+\infty} \sigma(v) v f(v, T_\parallel, T_\perp) d^3 v, \quad (4)$$

where $f(v, T_\parallel, T_\perp)$ is the anisotropic electron velocity distribution, which is characterized by the parallel and perpendicular electron temperatures $k_B T_\parallel = 0.8$ meV and $k_B T_\perp = 40$ meV (Huang et al. 2015).

4. Results and Discussion

4.1. Merged-beam Recombination Rate Coefficients

The absolute merged-beam recombination rate coefficients in the energy range 0–51.88 eV for Be-like calcium ions are displayed in Figure 1. It contains DR resonances associated with excitation of the $2s^2$ core to the $2s2p\ ^3P_{0,1,2}$ and $2s2p\ ^1P_1$ levels and significant TR contributions. The resonance

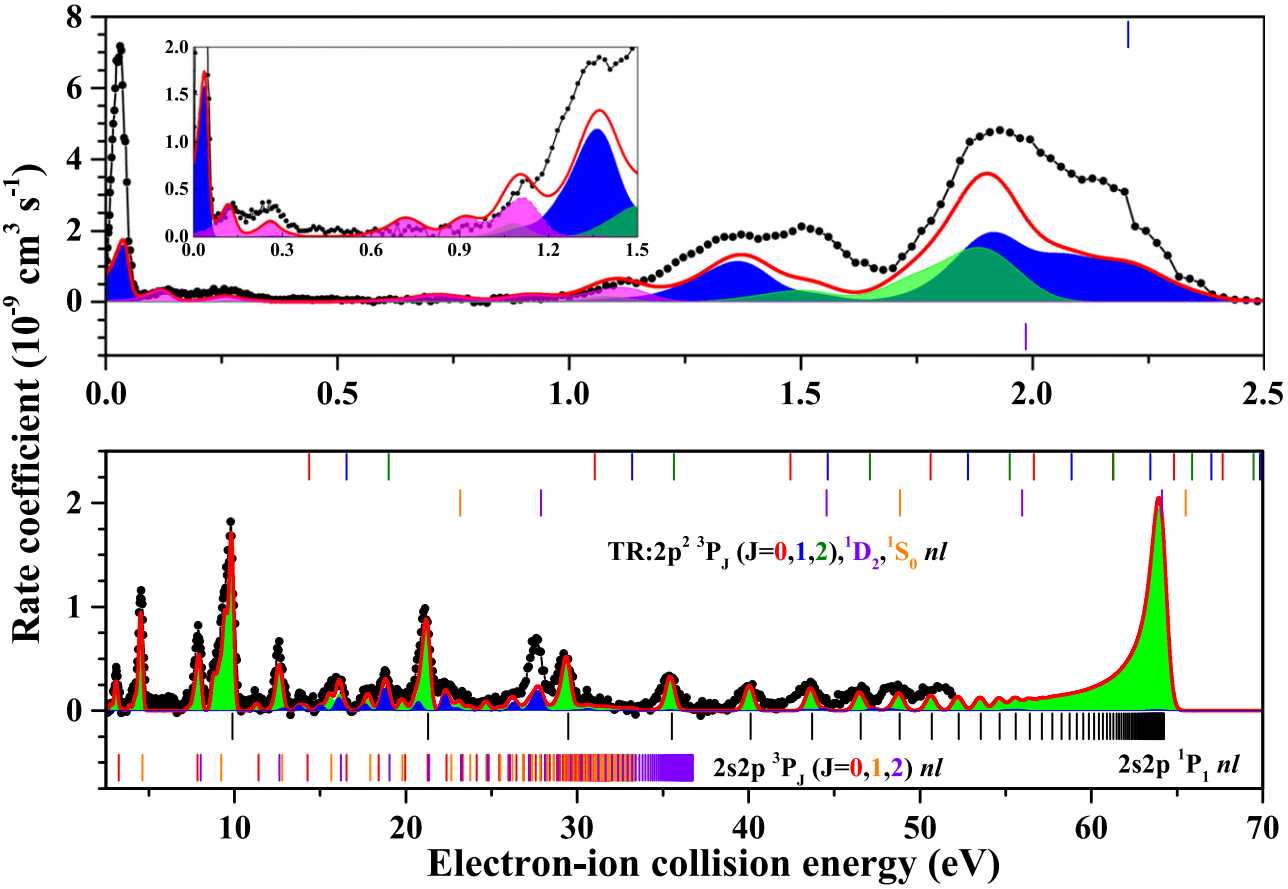

Figure 1. Measured and calculated recombination rate coefficients of Be-like Ca. The experimental result (the connected filled circles) covers the energy range of 0–51.88 eV. The presently calculated rate coefficient (the red solid line) accounts for fractions of 95% ground-state ions and 5% $2s2p\ ^3P_0$ metastable ions. The pink shaded area shows the rate coefficient originating from the metastable state ions. The shaded green and blue curves denote the calculated DR and TR rate coefficients, respectively. The vertical bars below the spectra denote the estimated resonance positions (Equation (5)) for the $\Delta N = 0$ series of DR resonances associated with $2s^2\ ^1S_0 \rightarrow 2s2p\ ^3P_{0,1,2},^1\ P_1$ core excitations. TR resonance positions associated with the $2s^2\ ^1S_0 \rightarrow\ 2p^2\ ^3P_{0,1,2},\ ^1D_2,\ ^1S_0$ core excitations are indicated by the differently colored vertical bars above the spectra.

positions can be estimated by the Rydberg formula

$$E_{\rm res}(n) = E_{\rm exc} - R\frac{q^2}{n^2}, \quad (5)$$

where $R \approx 13.60569$ eV is the Rydberg constant, $q = 16$ is the primary ion charge state, n denotes the principal quantum number of the captured electron, and $E_{\rm exc}$ is the core-excitation energy. Values for $E_{\rm exc}$ are listed in Table 1 for a number of transitions of interest. The formula works well for high-n resonances where the interaction between the Rydberg electron and the core electrons is very weak. However, the low-n resonance positions are dominated by the complex fine structure of the associated multiply excited configurations. The recombined ions will experience one toroidal magnet, three quadrupole magnets, and one dipole magnet on their way to the detector during this experiment. The motional electric fields that the ions experience in these magnets lead to field ionization of Rydberg electrons with their principal quantum numbers $n > n_{\rm cutoff}$ will be field-ionized at the magnets before being detected. The field-ionized ions cannot be separated from the primary ion beam and, consequently, will not be detected. The cut-off quantum number $n_{\rm cutoff}$ can be estimated by a simple formula (Fogle et al. 2005). However, the present experimental recombination spectrum does not cover high-n Rydberg levels converging to the $2s2p(^1P_1)$ series limit at 64.301 eV and the $2s2p(^3P_J)$ series limits at about 32–37 eV (Table 1) are not prominently visible, either, such that there are no marked field-ionization effects on the presently measured DR spectrum.

The green shaded area in Figure 1 denotes the calculated $2s^2 \rightarrow 2s2p\ \Delta N = 0$ DR rate coefficient. It can be found that the measured spectrum cannot be reproduced by the calculation that only takes DR into account (green shade curve), for example, the features below 50 meV and around 1.5, 2.2, and 27.5 eV. It can be seen from Figure 1 that the experimental features agree better with the solid red line that takes TR contributions into account. The first resonances situated below 50 meV, which can be attributed to TR, are significantly stronger than any other resonance feature in the spectrum. The resonance strengths of this feature and of those around 1.5, 2.2, and 27.5 eV, which are also dominated by TR, are all underestimated by the theoretical calculation. However, the calculated resonance positions fit with the experimental result well. Therefore, the discrepancies between the experimental rate coefficients and calculated result are mainly due to the underestimation of the TR resonance strengths. As described by Schnell et al. (2003), the formation of the intermediate levels depends sensitively on the details of configuration mixing, making the calculation of TR a challenge for atomic-structure theory.

As a Be-like $^{40}Ca^{16+}$ ion with zero nuclear spin, its $2s2p\ ^3P_0$ excited level can only decay to the ground-state by E1M1 two-photon transition (Marques et al. 1993; Cheng et al. 2008; Fritzsche et al. 2015). Correspondingly, the associated lifetime of this state is about 2.3×10^6 s, which is much longer than the experimental timescale. A fraction of the circulating ions in the storage ring were expected to be at the $2s2p\ ^3P_0$ level during the experiment. Ions in other excited levels can decay to the ground level during the electron cooling delay before the measurement since their lifetimes are rather short compared to the 2 s delay time (see Table 1). The fractions of the long-lived $^3P_0$ metastable level when extracted from an ECR ion source were discussed by Orban et al. (2011). Accordingly, the percentage of the metastable ions decreases with increasing charge state within the Be-like isoelectronic sequence. For example, metastable fractions of 60%, 40%, 35%, and 14% were found for C^{2+}, N^{3+}, O^{4+}, and Ne^{6+} ion beams, respectively. Since the $^{40}Ca^{16+}$ ion beam was also produced by an ECR ion source for this experiment, a fraction of 5% metastable calcium ions was estimated. This corresponds roughly to what was previously assumed for neighboring members of the Be-like isoelectronic sequence of ions such as Ar^{14+} (Huang et al. 2018) and Ti^{18+} (Schippers et al. 2007a). A separate calculation for the parent ions at the $2s2p\ ^3P_0$ level was also conducted. It is found that most of the resonance features below 1.25 eV are associated with DR of metastable parent ions. The pink shaded curve denotes the calculated rate coefficients for the 5% metastable ions. For an overall comparison with the experimental recombination spectrum shown in Figure 1, the rate coefficients for ground level and metastable ions were scaled to 95% and 5%, respectively. With this adjustment, the overall agreement between the experiment and theory is satisfactory except for the strong TR resonances as discussed above.

The overall uncertainty of the measured rate coefficients is estimated to be less than 30% (at a 1σ confidence level). It consists of a 15% uncertainty due to the statistics, the electron and ion beam current, the electron–ion interaction length, the background subtraction, an uncertainty of 5% from the estimated metastable content, and an uncertainty of 20% on account of the electron density distribution profile and the ion beam position in this profile.

4.2. Plasma Recombination Rate Coefficients (PRRCs)

For the applications in plasma modeling and astrophysics, PRRCs for the resonant recombination channels are needed. The temperature dependent PRRC $\alpha(T_e)$ can be derived by convoluting the RR-subtracted experimental recombination rate coefficient with a Maxwell–Boltzmann electron energy distribution of temperature T_e (Schippers et al. 2001):

$$\alpha(T_e) = \int \alpha(E) f(E, T_e) dE, \tag{6}$$

$f(E, T_e)$ is the electron energy distribution:

$$f(E, T_e) = \frac{2E^{1/2}}{\pi^{1/2}(kT_e)^{3/2}} \exp\left(-\frac{E}{kT_e}\right). \tag{7}$$

Temperature dependent PRRC derived from the experimental result and from the AUTOSTRUCTURE calculation are displayed in Figure 2. Since the presently measured rate coefficient misses the $^1P_1$ series limit, the measured electron–ion recombination rate coefficients from 42 to 70 eV were replaced by the field-ionization-free calculated results including the resonances with the free electron captured into a Rydberg level $n_{max} = 1000$. The contribution from the resonances into a Rydberg level with $n > 1000$ was small enough to be neglected safely. Such a derived plasma rate coefficient is called field-ionization-free PRRC. It is shown as a black solid line in Figures 2 and 3. To compare with the theoretical rate coefficients from the literature, the calculated metastable contribution was subtracted from the measured recombination

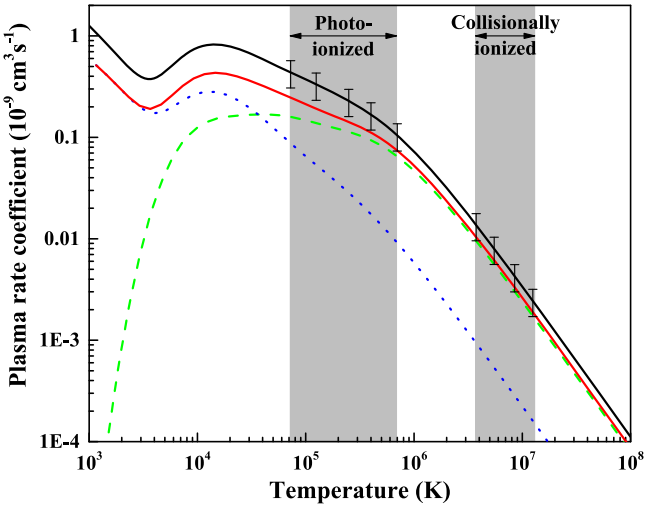

Figure 2. Electron temperature dependent plasma recombination rate coefficients for Be-like Ca. The experimentally derived (solid black line) and calculated (red solid line) rate coefficients contain the $\Delta N = 0$ DR and TR resonances. The green dashed line and blue dotted line denote the rate coefficients derived from the AUTOSTRUCTURE calculated DR and TR rates, respectively. The gray shaded areas and associated arrows indicate the temperature ranges where Ca^{16+} is most formed in PP and CP (Kallman & Bautista 2001; Bryans et al. 2009). The error bars denote a 30% experimental uncertainty.

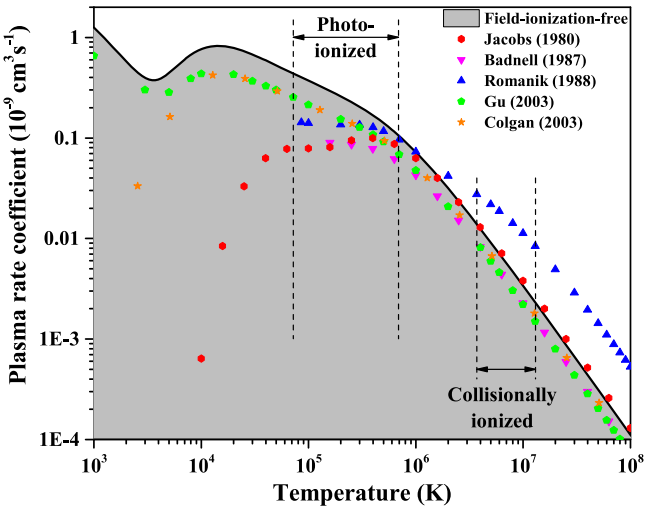

Figure 3. Comparison of the present field-ionization-free resonant plasma recombination rate coefficient (black solid line) with the available literature data for Be-like Ca. The rate coefficients calculated by Jacobs et al. (1980) and Badnell (1987) are displayed as red hexagons and magenta down-triangles, respectively. The calculations by Romanik (1988) and Gu (2003) are represented as blue up-triangles and green pentagons, respectively. The orange stars show the $\Delta N = 0$ DR and TR rate coefficients calculated by Colgan et al. (2003). The vertical dashed lines and associated arrows mark the temperature range where the abundance of Be-like Ca exceeds 10% of its maximum value in PP and CP (Kallman & Bautista 2001; Bryans et al. 2009).

Table 2
Fitted Parameters for the Resonant Recombination Channels Derived from the Experimental and Calculated Rate Coefficients

No.	Experiment		AUTOSTRUCTURE ($n_{max} = 1000$)	
i	c_i	E_i	c_i	E_i
1	5.0219	0.55388	3.6230	0.05795
2	6.1690	0.03800	47.571	1.3072
3	260.09	3.2522	151.74	4.8012
4	453.85	1.7154	257.92	2.0015
5	1193.7	9.2268	825.99	10.562
6	2916.7	23.188	1610.5	25.048
7	6298.3	57.720	5795.4	60.088

Note. The units of c_i and E_i are 10^{-5} cm^3 s^{-1} K$^{3/2}$ and eV, respectively.

rate coefficient. The remaining rate coefficient was then renormalized to a 100% ground-level ion beam by dividing it by a factor of 0.95. The dashed and dotted lines in Figure 2 show the DR and TR contributions, respectively. The vertical error bars denote the 30% uncertainty of the measured recombination rate coefficient.

The temperature range in Figure 2 is from 10^3 K to 10^8 K including the ranges where Be-like Ca forms in PP and CP. The gray shaded areas with associated arrows indicate these temperature ranges. The boundaries of these bands correspond to the temperatures where the fractional abundance of Be-like Ca is 10% of its maximum value (Kallman & Bautista 2001; Bryans et al. 2009). TR resonances dominate the rate coefficient for temperatures below 3.5×10^4 K. They play an important role in PP, while the TR contribution to the rate coefficient is less than 10% in the temperature range of CP. For temperatures below 5.5×10^4 K, where the TR contribution is higher than 40%, the deviation between the experimentally derived PRRC and the AUTOSTRUCTURE calculation is more than 45%. Over the temperature range of PP, this deviation decreases from 45% to 30% with the decline of the TR contribution. An agreement of better than 25%, i.e., within the experimental uncertainty is found between the present experimental result and the AUTOSTRUCTURE calculation in the collisionally ionized temperature range. A reasonable explanation is that the theoretical calculation underestimates the resonance strengths below 50 meV, around 1.5, 2.2, and 27.5 eV.

For a convenient use of our data in plasma modeling codes, the presently derived PRRC were fitted with the function:

$$\alpha(T_e) = T_e^{-3/2} \sum_i c_i \exp\left(-\frac{E_i}{kT_e}\right). \quad (8)$$

The fitted values of c_i and E_i are listed in Table 2. The fitted results reproduce the data to within 1% across the entire temperature range of Figure 2. The fitted parameters resulting from the AUTOSTRUCTURE calculation are also presented.

In Figure 3, the experimentally derived field-ionization-free PRRC are compared with the theoretically calculated ones from the literature. Results of Jacobs et al. (1980) and Romanik (1988) include DR associated with the $\Delta N = 0$ and $\Delta N = 1$ core transitions. Romanik declared that their results may be incomplete below 8.5×10^4 K for Be-like Ca due to the omission or energy uncertainty of resonances (Romanik 1988). Calculation of $\Delta N = 0$ and $\Delta N = 1$ DR had also been performed by Badnell (1987) and collected by Mazzotta et al. (1998), here we simply present the calculated rate coefficient of $\Delta N = 0$ DR. Theoretical calculations by Gu (2003) with the FAC code and by Colgan et al. (2003) with the AUTOSTRUCTURE code provided rate coefficients of $\Delta N = 0$ DR and TR for temperatures from 10^3 K to 10^8 K. It should be noted that the data of Colgan et al. (2003) as shown in Figure 3 is the revised $\Delta N = 0$ rate coefficients from the OPEN-ADAS[8] website.

For temperatures below 5×10^4 K the calculated PRRC by Gu (2003) and Colgan et al. (2003) are more than 45% lower than the experimentally derived one. A probable reason is that the predictions of the low-temperature DR and TR rate coefficients are not reliable. The data of Jacobs et al. (1980) are even lower for these temperatures since TR was not included in the calculations. At temperatures of about 4×10^5 K, where Be-like Ca is most abundant in PP, the calculated rate coefficients by Gu (2003) and Colgan et al. (2003) are 35% lower than the experimental result. Rate coefficient calculated by Badnell (1987) is about 50% lower than the experimental result since TR was not included in the calculation. The deviation of the theoretical calculated rate coefficients from the experimental results is probably due to the fact that the TR resonances and the low-temperature DR resonances cannot be calculated with sufficient precision. In the temperature range of 4×10^6–1.3×10^7 K, Be-like Ca is formed in CP such as solar strong active regions and flares in the upper solar atmosphere. In this temperature range, the calculated data by Badnell (1987) and Gu (2003) are about 35% lower than the experimental result. An agreement of better than 25% was found between the experimentally derived PRRC and the calculation by Colgan et al. (2003). The calculated data of Jacobs et al. (1980) and Romanik (1988) are higher than the experimental data. This is mainly because their calculation included the $\Delta N = 0$ and $\Delta N = 1$ DR, while the experimentally derived PRRC only include the resonant recombination associated with $\Delta N = 0$ core excitations. The contribution from $\Delta N = 1$ DR cannot be neglected for CP, by 5×10^6 K it is larger than the $\Delta N = 0$, and was accounted-for by Colgan et al. (2003), for example.

5. Conclusion

Absolute electron–ion recombination rate coefficients of Be-like $^{40}Ca^{16+}$ have been measured at the CSRm in the energy range of 0–51.88 eV. In addition, theoretical results from the AUTOSTRUCTURE code are presented and compared with the present experimental results. Good agreement was found between calculation and experiment as far as DR resonances are concerned. However, the calculated TR resonance strengths underestimate the experimental ones, and this translates into a deviation between the experimental and theoretical plasma rate coefficients exceeding the experimental uncertainty. Several resonances originating from the long-lived $2s2p\ ^3P_0$ metastable ions have been identified in the measured spectrum. The calculation for 95% of ions in the ground state and 5% of ions in the metastable state agrees well with the experimental results for these resonances. The present investigation indicates that the calculation of TR resonances is still a challenging task for the state-of-the-art ATUOSTRUCTURE code, while the DR resonances can be calculated with reasonably high precision.

[8] http://open.adas.ac.uk/

Experimentally derived field-ionization-free temperature dependent PRRC were presented and compared with the available theoretical results. The experimentally derived PRRC are higher than the theoretical data in the photoionized zone where TR resonances are important. In a CP, where Ca^{16+} is most abundant in solar active region and flares, the rate coefficients are dominated by DR resonances, and an agreement of better than 25% is found between the present experimental result and the more recent calculation by Colgan et al. (2003) and the present AUTOSTRUCTURE calculation. Our result provides benchmark recombination data of Ca^{16+} for plasma modeling in astrophysics.

This work is partly supported by the National Key R&D Program of China under grant No. 2017YFA0402300, the National Natural Science Foundation of China through No. 11320101003, No. U1732133, No. 11611530684, the Strategic Priority Research Program of the Chinese Academy of Sciences, grant No. XDB21030300 and the Key Research Program of Frontier Sciences, CAS, grant No. QYZDY-SSW-SLH006. W.Q.W acknowledges the support by the Youth Innovation Promotion Association of the Chinese Academy of Sciences. S.P.P. and N.R.B. acknowledge the support of EPSRC grant EP/L021803/1. S.S. gratefully acknowledges support by the CAS Presidents International Fellowship Initiative (PIFI). The authors would like to thank the crew of the Accelerator Department for skillful operation of the CSR accelerator complex.

ORCID iDs

W. Q. Wen https://orcid.org/0000-0001-5266-3058
S. Schippers https://orcid.org/0000-0002-6166-7138
X. Ma https://orcid.org/0000-0001-9831-0565
L. F. Zhu https://orcid.org/0000-0002-5771-0471

References

Ali, S., Orban, I., Mahmood, S., Loch, S. D., & Schuch, R. 2013, A&A, 557, A2
Asplund, M., Grevesse, N., Sauval, A. J., & Scott, P. 2009, ARA&A, 47, 481
Badnell, N. R. 1987, JPhB, 20, 2081
Badnell, N. R. 2007, JPhCS, 88, 012070
Badnell, N. R. 2011, CPC, 182, 1528
Beiersdorfer, P. 2003, ARA&A, 41, 343
Bernhardt, D., Becker, A., Brandau, C., et al. 2016, JPhB, 49, 074004
Bernhardt, D., Brandau, C., Harman, Z., et al. 2015, JPhB, 48, 144008
Beyer, H. F., & Shevelko, V. P. 2003, Series in Atomic and Molecular Physics: Introduction to the Physics of Highly Charged Ions (Bristol: Institute of Physics Publishing)
Brandau, C., Kozhuharov, C., Lestinsky, C., et al. 2015, PhS, T166, 014022
Bryans, P., Landi, E., & Savin, D. W. 2009, ApJ, 691, 1540
Burgess, A. 1964, ApJ, 139, 776
Cheng, K. T., Chen, M. H., & Johnson, W. R. 2008, PhRvA, 77, 052504
Colgan, J., Pindzola, M. S., Whiteford, A. D., & Badnell, N. R. 2003, A&A, 412, 597
Danared, H. 1993, NIMA, 335, 397
Decourchelle, A., Sauvageot, J. L., Audard, M., et al. 2001, A&A, 365, L218
Doschek, G. A., & Feldman, U. 2010, JPhB, 43, 232001
Feldman, U., & Laming, J. M. 2000, PhS, 61, 222
Fogle, M., Badnell, N. R., Glans, P., et al. 2005, A&A, 442, 757
Fritzsche, S., Surzhykov, A., & Volotka, A. 2015, NJPh, 17, 103009
Gu, M. F. 2003, ApJ, 590, 1131
Huang, Z. K., Wen, W. Q., Wang, H. B., et al. 2015, PhS, T166, 14023
Huang, Z. K., Wen, W. Q., Xu, X., et al. 2017, JPhCS, 875, 012020
Huang, Z. K., Wen, W. Q., Xu, X., et al. 2018, ApJS, 235, 2
Hwang, U., & Laming, J. M. 2003, ApJ, 597, 362
Jacobs, V., Davis, J., Rogerson, J., et al. 1980, ApJ, 239, 1119
Kallman, T., & Bautista, M. 2001, ApJS, 133, 221
Kallman, T. R., & Palmeri, P. 2007, RMP, 79, 79
Keenan, F. P., Pinfield, D. J., Woods, V. J., et al. 1998, ApJ, 503, 953
Khan, N., Huang, Z. K., Wen, W. Q., et al. 2018, CPC, 42, 064001
Ko, Y.-K., Doschek, G. A., Warren, H. P., & Young, P. R. 2009, ApJ, 697, 1956
Kramida, A., Ralchenko, Yu., Reader, J. & NIST ASD Team 2018, NIST Atomic Spectra Database (ver. 5.5.2), https://physics.nist.gov/asd
Landi, E., & Bhatia, A. K. 2009, ADNDT, 95, 155
Lippmann, S., Finkenthal, M., Huang, L. K., et al. 1987, ApJ, 316, 819
Marques, J. P., Parente, F., & Indelicato, P. 1993, PhRvA, 47, 929
Mazzotta, P., Mazzitelli, G., Colafrancesco, S., & Vittorio, N. 1998, A&AS, 133, 403
Orban, I., Böhm, S., Loch, S. D., & Schuch, R. 2008, A&A, 489, 829
Orban, I., Loch, S. D., Böhm, S., & Schuch, R. 2010, ApJ, 721, 1603
Orban, I., Loch, S. D., Glans, P., Böhm, S., & Schuch, R. 2011, PhS, T144, 014035
Orlov, D. A., Krantz, C., Bernhardt, D., et al. 2009, JPhCS, 163, 012058
Paerels, F. B., & Kahn, S. M. 2003, ARA&A, 41, 291
Romanik, C. J. 1988, ApJ, 330, 1022
Savin, D., Gwinner, G., Grieser, M., et al. 2006, ApJ, 642, 1275
Savin, D. W. 2007, JPhCS, 88, 012071
Schippers, S. 2012, JPhCS, 388, 012010
Schippers, S. 2015, NIMB, 350, 61
Schippers, S., Bartsch, T., Brandau, C., et al. 2000, PhRvA, 62, 022708
Schippers, S., Bernhardt, D., Müller, A., et al. 2012, PhRvA, 85, 012513
Schippers, S., Müller, A., Gwinner, G., et al. 2001, ApJ, 555, 1027
Schippers, S., Schmidt, E. W., Bernhardt, D., et al. 2007a, JPhCS, 58, 137
Schippers, S., Schmidt, E. W., Bernhardt, D., et al. 2007b, PhRvL, 98, 033001
Schippers, S., Schnell, M., Brandau, C., et al. 2004, A&A, 421, 1185
Schnell, M., Gwinner, G., Badnell, N. R., et al. 2003, PhRvL, 91, 043001
Schuch, R., & Böhm, S. 2007, JPhCS, 88, 012002
Wang, K., Guo, X. L., Liu, H. T., et al. 2015, ApJS, 218, 16
Wen, W. Q., Ma, X., Xu, W. Q., et al. 2013, NIMB, 317, 731